Impact of Membrane Protein–Lipid Interactions on Formation of Bilayer Lipid Membranes on SAM-Modified Gold Electrode

Masaru Kato,[a,b,c,*] *Yuya Masuda,*[b] *Narumi Yoshida,*[b] *Takehiko Tosha,*[d] *Yoshitsugu Shiro,*[e] *Ichizo Yagi*[a,b,c,*]

[a] Faculty of Environmental Earth Science and [b]Graduate School of Environmental Science, Hokkaido University, N10W5, Kita-ku, Sapporo 060-0810, Japan.

[c]Global Research Center for Environment and Energy based on Nanomaterials Science (GREEN), National Institute for Materials Science (NIMS), Tsukuba 305-0044, Japan.

[d]RIKEN SPring-8 Center, Kouto, Sayo, Hyogo 679-5148, Japan.

[e]Graduate School of Life Science, University of Hyogo, Hyogo 678-1297, Japan.

Corresponding authors

*E-mail: masaru.kato@ees.hokudai.ac.jp (MK); iyagi@ees.hokudai.ac.jp (IY)

Highlights

- A protein-tethered bilayer lipid membrane (ptBLM) was assembled on SAM/Au.

- The ptBLM assembly was monitored by time-resolved SEIRA spectroscopy.

- The lipid bilayer formation kinetics was influenced by protein–lipid interactions.

- Protein–lipid interactions improved the electrocatalytic stability of the cNOR.

Graphical abstract

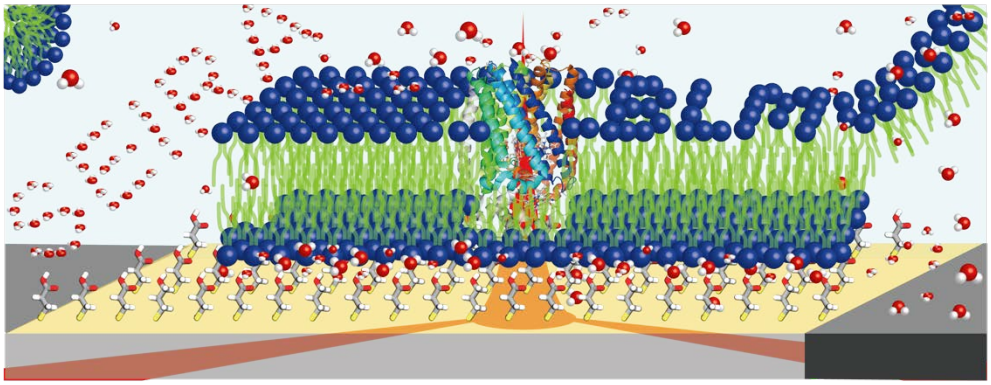

Keywords

Membrane protein, surface-enhanced infrared absorption spectroscopy, nitric oxide reductase, protein-tethered bilayer lipid membrane, protein film electrochemistry.

Abstract

In protein film electrochemistry for redox-active membrane proteins, the reconstitution of protein-tethered bilayer lipid membranes (ptBLMs) can maximize their functionality and stability at electrolyte/electrode interfaces. To understand the impact of protein–lipid interactions on the ptBLM formation, we tracked the reconstitution process of a lipid bilayer in the presence or the absence of a transmembrane enzyme of cytochrome *c*-dependent nitric oxide reductase (cNOR) on a mixed self-assembled monolayer (SAM)/Au electrode. Time-resolved surface-enhanced infrared absorption (SEIRA) spectroscopy and electrochemical measurements revealed that the protein–lipid interaction affected the formation kinetics for the phospholipid bilayer and the electrocatalytic stability of the cNOR-modified electrode but not the fluidity of the phospholipid bilayer.

1. Introduction

Membrane proteins show important biological functions in lipid membranes including transmembrane transport of electrons, ions, and small molecules, signal transduction, and enzymatic activity [1-4]. They are evolutionally optimized to show high activity and stability in lipid membranes. However, relatively large multi-subunits with hydrophobic and hydrophilic domains of membrane proteins decrease the protein stability, and therefore biomimetic studies of membrane proteins are still challenging. Particularly, biomimetic studies on redox-active transmembrane proteins and enzymes give us mechanistic insights into their functions and stability, leading us to develop bio-based or bio-inspired devices related to medicine, sensing, and sustainable energy production [5,6].

Protein film electrochemistry (PFE) is a powerful technique to understand the electrochemical behavior of redox-active proteins including membrane enzymes [6-11]. In PFE, target proteins are immobilized on conductive electrode materials such as noble metals including gold [12-16], carbon [17,18] and metal oxides [19-22]. To preserve the native function of membrane proteins even on electrode surfaces in PFE, electrode

surfaces are often coated with self-assembled monolayers (SAMs) before the immobilization of the protein on the electrode [7,12-15,19]. For membrane proteins, lipid bilayers are constructed at the liquid/solid (electrolyte/electrode) interface to form protein-tethered bilayer lipid membranes (ptBLMs) [10,23-27], where protein–lipid interactions are expected to regulate properties of ptBLMs including the formation kinetics, membrane fluidity, electrocatalytic activity, and stability. Since the ptBLM formation occurs at the electrolyte/electrode interfaces, even these fundamental properties on ptBLMs are still not well understood.

Herein, we investigated the influence of protein–lipid interactions on the formation kinetics, membrane fluidity, electrocatalytic activity, and stability of a ptBLM at the electrolyte/electrode interface in the presence or absence of a transmembrane metalloenzyme of cytochrome *c*-dependent nitric oxide reductase (cNOR) from *P. aeruginosa*. The cNOR catalyzes the reduction of lethal nitric oxide (NO) to nitrous oxide (N_2O) in not only the biological denitrification process but also electrochemical conditions [12,17,28,29]. NO is an important intermediate to achieve the selective electrochemical nitrate reduction to dinitrogen [30] and therefore the electrochemical

studies on the cNOR would enable us to understand the enzymatic machinery as well as design artificial electrocatalysts for the selective NO reduction. In this work, the cNOR was immobilized on a SAM-coated gold electrode and then the ptBLM with a phospholipid of 1,2-Dimyristoyl-*sn*-glycero-3-phosphocholine (DMPC) was constructed by surfactant–lipid exchange. The ptBLM formation process was tracked by time-resolved surface-enhanced infrared absorption (SEIRA) spectroscopy. SEIRA spectroscopy is a surface-sensitive technique and used to distinguish specifically adsorbed (bio)molecules from the nonspecifically adsorbed ones [6,8,23,25,31-38]. In this work, the time-resolved SEIRA spectroscopy was applied to study molecular dynamics on the ptBLM assembly of the cNOR and DMPC on the SAM/Au electrode.

2. Experimental section

2.1. Materials

Chemicals and gases were purchased from the following companies and used without further purification: 1-ethyl-3-(3-dimethylaminopropyl)carbodiimide hydroxide (EDC, ≥98%), 2-morpholinoethanesulfonic acid (MES-H) monohydrate (≥99%), and n-dodecyl-β-D-maltoside (DDM, ≥98%) from Dojindo Molecular Technologies; sodium 2-

morpholinoethanesulfonate (MES-Na, ≥97%) and 3-mercapto-1-propanol (MPL, ≥97%) from Tokyo Chemical Industry; Bio-beads SM-2 adsorbent media from BIO-RAD; ultrapure Ar (99.999%) from Hokkaido Air Water; 50% nitric oxide (NO) in Ar from Tomoe Shokai; DMPC (≥99%), K_2SO_4 (≥99%), NaOH (≥97%), $NaAuCl_4 \cdot 2H_2O$ (≥95%), NH_4Cl (≥99%), hydrofluoric acid solution (46%), hydrochloric acid solution (35~37%), and sulfuric acid solution (96~98%) from FUJIFILM Wako Pure Chemical; deuterium oxide (D_2O, ≥99.9%) from ISOTEC; 3-mercaptopropionic acid (MPA, ≥99%), *N*-hydroxysuccinimide (NHS, ≥98%), and sulfuric acid-d_2 solution (D_2SO_4, 96−98wt% in D_2O, 99.5 atom%D) from Sigma-Aldrich; Na_2SO_3 (≥97%) and $Na_2S_2O_3 \cdot 5H_2O$ (≥99%) from Kanto Chemical Co., inc.; nitric acid solution (60%) from Junsei Chemical, Ltd.; ammonium fluoride solution (40%) from Morita Chemical Industries. To determine pD values of solutions in D_2O, pH values were measured with a glass electrode (9615S-10D Standard ToupH electrode, LAQUA, HORIBA) and then converted into pD values by adding 0.41 [39]. The cNOR was isolated and purified from *P. aeruginosa* according to the literature [40,41].

2.2 Preparation of SEIRA-active Au thin-films on Si (Au/Si) prisms

SEIRA-active Au thin-films on half-cylindrical Si prisms (Pier Optics Co., Ltd.) were prepared based on the previously reported procedure [12,42-44]. The prism surface was polished on a polishing pad (BAS) with alumina powder suspension (1 μm, Baikalox) and then polished with paper (Prowipe S200, Elleair) in running tap water until the surface became hydrophilic. The prism was sonicated in Milli-Q water twice, acetone and then Milli-Q water for 5 min each to completely remove alumina from the Si surface. The cleaned Si surface was contacted with 40% NH_4F aq. For 90 s to remove surface oxide and then rinsed with Milli-Q water. The Si prism was heated on a hot plate at 70ºC until the electroless gold deposition. A plating solution was prepared as follows: 1 mL of 0.03 M $NaAuCl_4$ aq. was added to 1 mL of an aqueous solution containing 0.3 M Na_2SO_3, 0.1 M $Na_2S_2O_3$ and 0.1 M NH_4Cl, 1 mL of 2 vol% HF aq. was added to the mixture, and then the obtained plating solution was heated on the hot plate at 70ºC. After 15 min, ca. 1.5 mL of the plating solution was drop-cast on the Si prism surface and kept for ca. 1 min to obtain a gold film. The gold film was removed with ca. 200 μL of aqua regia and then the Si surface was rinsed with Milli-Q water. A gold film was deposited on the Si prims in the same manner again. The gold film deposition was repeated several times

until a resistance of the gold film reached to 10 to 20 Ω, which was checked by using a multimeter.

2.3. Self-assembly of a mixed monolayer of alkanethiols on the SEIRA-active Au/Si prism

A mixed SAM of MPA and MPL with a 3:1 molar ratio was prepared on the SEIRA-active Au/Si prism. The surface of a Au/Si prism was electrochemically cleaned: the Au/Si prism was used as the working electrode and five potential cycles were performed at a sweep rate of 30 mV s^{-1} in the potential range from +0.1 to +1.45 V vs. Ag|AgCl (sat. KCl) in a 0.1 M H_2SO_4 aqueous solution under Ar. Based on the charges of the reduction of the surface oxide in cyclic voltammograms, roughness factors were determined to be 2.6 to 3.5, assuming 420 μC cm^{-2} for the reduction of the Au surface oxide [12]. Since the geometrical surface area of the Si prism is 2.0 cm^2, electrochemically active surface areas of the Au film were calculated to be 5.2 to 7.0 cm^2. After the electrochemical cleaning process, the surface of the Au/Si prism was rinsed with ca. 15 mL of Milli-Q water five times and then ca. 15 mL of ethanol five times. To prepare the mixed SAM on Au (SAM/Au), the cleaned Au/Si prism surface was covered with a 4 mL ethanolic solution

containing 0.75 mM MPA and 0.25 mM MPL and then kept for 15 h under Ar in the dark. The surface was rinsed with ethanol to remove physically adsorbed alkanethiols.

2.4. Immobilization of cNOR on SAM/Au film

Onto the SAM/Au, 276 μL of the 20 mM MES-buffered solution in D_2O at pD 6.5, which was prepared from MES-Na and 5 M D_2SO_4 solution in D_2O, was drop-cast, and then the mixture of 3 μL of a 50 μM cNOR solution and 179 μL of the 20 mM MES solution containing 0.1 wt% DDM were added by drop-casing. After keeping the solution-covered film in the dark for 20 min, 99 μL of the 20 mM MES-buffered solution containing 21 mM EDC and 83 μL of the 20 mM MES-buffered solution containing 14 mM NHS were added on the SAM/Au film. After keeping the solution-covered film in the dark for 90 min, the surface was carefully rinsed with the 20 mM MES solution in D_2O to obtain the Au film covalently modified with cNOR *via* the mixed SAM.

2.5. Bilayer lipid membrane (BLM) assembly on SAM/Au in the absence of cNOR

DMPC (1 mg mL^{-1}) and DDM (0.1 wt%) were dissolved in the 20 mM MES-buffered aqueous solution at pH 6.5, which was prepared from MES-H, Milli-Q water, and 5 M NaOH aq. The MES-buffered solution was kept in an ice bath under ultrasonication for

at least 2 h until the DDM and DMPC were completely dissolved into the solution. The prepared solution was kept in a refrigerator until use. The cold DDM–DMPC solution (1 mL) was drop-cast onto the SAM/Au film and then 50 mg of Bio-beads were added to the solution twice.

2.6. Assembly of protein-tethered BLM (ptBLM)

The experimental procedure on the assembly of the ptBLM is the same as that for the BLM/SAM/Au except for the use of cNOR–SAM/Au film.

2.7. SEIRA spectroscopy measurements.

SEIRA spectra were recorded on a Varian 7000 FT-IR spectrometer equipped with a HgCdTe detector (MCT), which was cooled with liquid nitrogen during the measurements. A polarization controller (SP01, Sankei Technics) and an infrared polarizer (GS12000, SPECAC) were used in front of the sample to obtain *s*- and *p*-polarized light beams [45], where *s*- and *p*-polarized spectra were recorded and the *s*-polarized spectrum was used as the background to minimize signals originating from the bulk solution and maximize the signal intensity of the electrode surface. The polarization-modulated absorbance is defined as $A = -\log(I_p/I_s)$, where I_p and I_s are the single-beam intensities of the reflected

p- and *s*-polarized infrared radiation, respectively. Differential spectra were obtained as $A_{sample} - A_{ref}$, where A_{sample} and A_{ref} are polarization-modulated absorbances for the sample and reference, respectively. The SEIRA-active Au thin film on the prism that was attached to a home-made electrochemical glass cell was placed in the ATR Kretchmann configuration in the spectrometer. Each spectrum consists of 1024 interferograms, collected with a spectral resolution of 4 cm^{-1}.

2.8. Electrochemical measurements.

All electrochemical measurements were performed using home-made electrochemical glass cells with the three-electrode configuration. An aqueous electrolyte solution containing 50 mM MES and 50 mM K_2SO_4 in D_2O at pD 6.5 was used as the electrolyte solution. A platinum black-flag electrode and a Ag|AgCl (sat. KCl) electrode were used as the counter electrode and reference electrode, respectively. All potentials in the text were converted to SHE by adding +0.199 V to the potential vs. Ag|AgCl (sat. KCl).

For linear sweep measurements, the 50 mM MES-buffered electrolyte solution in D_2O containing 50 mM K_2SO_4 (pD 6.5) was purged with Ar for at least 1 h to remove oxygen, and then cyclic voltammograms of cNOR-modified Au electrodes were recorded for three

cycles in the potential range between –0.6 and +0.4 V vs. SHE at 20 mV s^{-1} under Ar. The electrolyte solution was purged with 50% NO/Ar at 3 sccm for 30 min and then cyclic voltammograms under 50% NO/Ar were recorded for 20 cycles in the potential range between –0.6 and +0.4 V vs. SHE at 20 mV s^{-1} under 50% NO/Ar. After that, the electrolyte solution was purged with 50% NO/Ar at 3 sccm for 3 min, and then the cyclic voltammogram, which is shown in the text, was recorded at 20 mV s^{-1} under 50% NO/Ar. To use the 50% NO/Ar gas, the NO/Ar gas was passed through 3 M NaOH aqueous solution (500 mL) twice, which removes NO_x, followed by Milli-Q water (500 mL) before introduced to the electrochemical cell. Both solutions were purged with Ar for at least 1 h before flowing the NO/Ar gas.

3. Results and discussion

3.1. Tracking of immobilization process of nitric oxide reductase on SAM/Au

The prepared SEIRA-active gold film on a polished Si hemisphere was coated with a mixed SAM of alkanethiols, 1:3 MPL−MPA, where thiol groups react with gold surfaces to form Au–S bonds, and terminal hydroxyl (-OH) and carboxylic acid (-COOH) groups are exposed to the solution (**Fig. 1**). Hydrophilic head groups of

carboxylate can provide protein anchoring sites *via* amide bonds [12,19] and hydroxyl groups can form a water-rich lubricant layer, which is known to improve the fluidity of supported BLMs [11]. Mixed-thiol SAMs are also known to increase the interfacial electron transfer rate for redox proteins immobilized on electrodes [46-51].

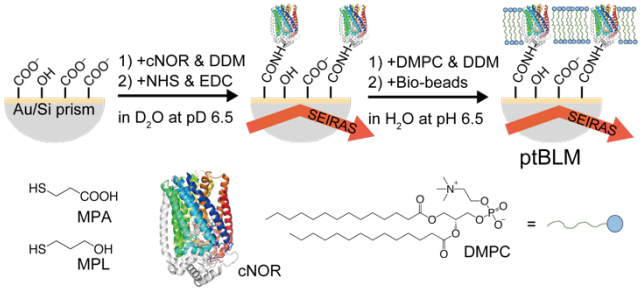

Fig. 1 Schematic representation of the preparation procedure of ptBLM of cNOR and DMPC. The SEIRA active gold film on the Si hemisphere (Au/Si) was coated with the mixed SAM of the 1:3 MPL–MPA mixture.

The protein immobilization process for the cNOR on the SAM-coated gold substrate was tracked by time-resolved SEIRA spectroscopy (**Fig. 2**). We observed characteristic amide I and amide II bands, which correspond to the C=O stretching mode at 1650 cm^{-1} and the C−N stretching and N−H bending modes at 1460 cm^{-1} (in D_2O), respectively [52]. The peak intensities of amide I and amide II bands increased during the cNOR

immobilization process, indicating that the successful immobilization of the cNOR on the SAM/Au.

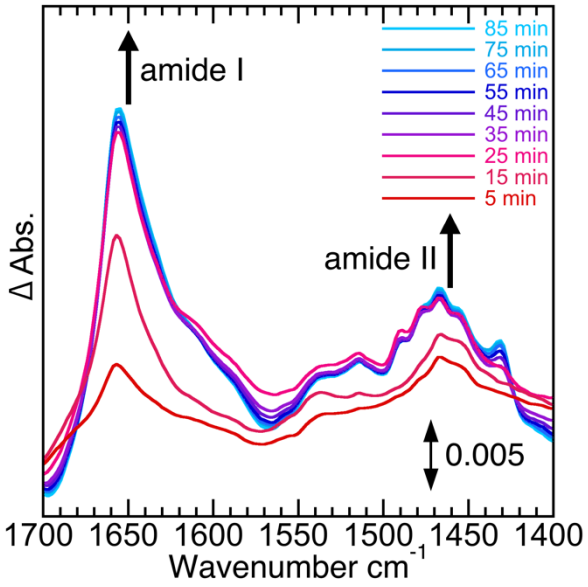

Fig. 2 Time-resolved SEIRA spectra of the cNOR immobilized on the mixed SAM of 1:3 MPL–MPA recorded in MES-buffered D_2O at pD 6.5. A polarization-modulated spectrum recorded in the absence of cNOR in solution was used as the reference spectrum.

SEIRA spectroscopy has an important feature of surface selection rule. Vibrational modes with dipole moment perpendicular to the SEIRA-active surface are strongly enhanced whereas those parallel to the surface are weakened. In SEIRA spectroscopy,

molecules adsorbed to the surface of SEIRA-active surfaces obey the surface selection rule and therefore some vibrational bands can appear with different intensities in the SEIRA spectrum as compared to the conventional IR spectrum. The comparison of relative band intensities also allows us to discuss the surface orientation of adsorbed molecules [31].

Peak intensity ratios of amide I to amide II ($\Delta I_{\text{amide I}}/\Delta I_{\text{amide II}}$) in the SEIRA spectra were determined to understand the protein orientation on the mixed SAM. The amide I mode of the α-helix is parallel to the helix axis whereas the amide II mode is perpendicular to it [27,52]. Since the cNOR has 13 α-helices that span the transmembrane region in the plasma membrane [53], $\Delta I_{\text{amide I}}/\Delta I_{\text{amideII}}$ values allowed us to understand the protein orientation of the cNOR on the SAM/Au: the α-helices adopt a more upright orientation (vertical to the surface) leading to increases in $\Delta I_{\text{amide I}}/\Delta I_{\text{amide II}}$ whereas the α-helices are parallel to the surface with decreasing $\Delta I_{\text{amide I}}/\Delta I_{\text{amide II}}$ values [12]. A $\Delta I_{\text{amide I}}/\Delta I_{\text{amide II}}$ value of the cNOR/SAM/Au at 90 min was determined to be 2.2. Since this value is higher than that previously obtained from a conventional IR spectrum of the cNOR in solution ($\Delta I_{\text{amide I}}/\Delta I_{\text{amide II}} = 1.6$), α-helices of the cNOR were

vertically oriented to the surface of SAM/Au (**Fig. 1**). The determined $\Delta I_{\text{amide I}}/\Delta I_{\text{amide II}}$ value was also higher than that for the cNOR immobilized on the SAM of MPA on gold (1.8–1.9) [12], suggesting that the protein orientation depends on terminal functional groups of alkanethiols used for the SAM [46,48] and the cNOR on the mixed SAM of MPA and MPL is more vertically oriented to the surface than that on the MPA SAM.

3.2. Tracking of ptBLM formation process

The formation process of the ptBLM on the mixed SAM was tracked by time-resolved SEIRA spectroscopy. The cNOR/SAM/Au film was placed in the MES-buffered aqueous solution at pH 6.5 containing DMPC and DDM. DDM works as a surfactant to solubilize DMPC in solution, and can be removed with bio-beads by surfactant–lipid exchange, leading to the reconstitution of the lipid bilayer of DMPC on the surface (**Fig. 1**) [13,25].

In the time-resolved SEIRA spectra, an increase of a strong, broad negative-going band was observed at ca. 3400 cm^{-1} (**Fig. 3a**). This band is associated with the OH stretching mode, ν(OH), of water molecules in a network of hydrogen bonds [54]. The increase of

negative ν(OH) band indicates that water molecules that were placed at the electrolyte/gold interface moved away during the ptBLM assembly. Three positive-going bands were also observed at ca. 2960, 2930, and 2860 cm^{-1} (**Fig. 3b**), which are associated with the asymmetric stretching of methyl groups, $\nu_{as}(CH_3)$, asymmetric stretching of methylene groups, $\nu_{as}(CH_2)$, and symmetric stretching of methylene groups, $\nu_s(CH_2)$, of DMPC, respectively [13,23,33,37,38]. The positive increase of these bands is a typical feature of the formation of tethered lipid bilayers [23,37,38]. Peak shifts to lower wavenumbers by ~3 cm^{-1} were also observed for the $\nu_{as}(CH_2)$ and $\nu_s(CH_2)$ bands after the surfactant–lipid exchange. Such peak shifts could be caused by orientational changes of methylene groups of DMPC from the *gauche* form to the *trans* form [38,55,56]. In other words, packing densities of the lipid bilayer of DMPC changed before and after the surfactant–lipid exchange [38,56].

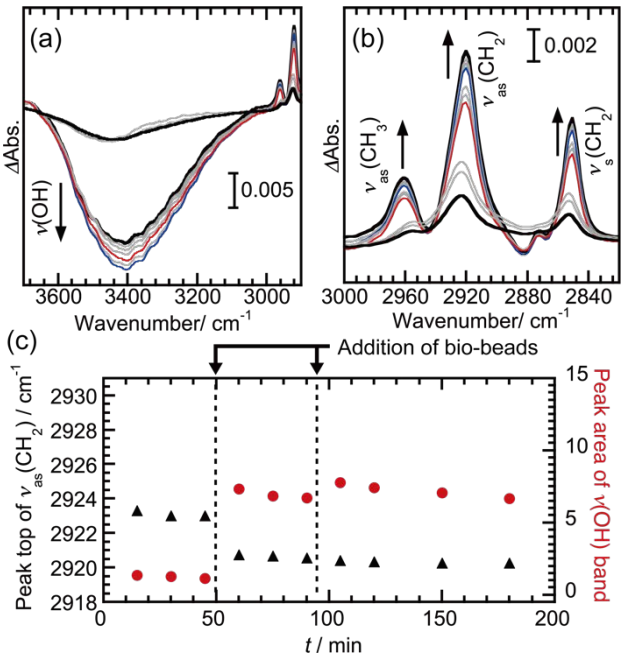

Figure 3. Differential SEIRA spectra of the ptBLM formation on the cNOR/1:3 MPL–MPA mixed SAM/Au (a) in the OH stretching region and (b) in the CH_3 and CH_2 stretching region. The traces in red and blue show the spectra just after the first and second additions of bio-beads, respectively. (c) Time course of the peak top position of the CH_2 stretching vibration mode and the peak area of OH stretching band. DMPC was added into the solution at t = 0 min and Bio-beads were added at t = 50 and 95 min. A polarization-modulated spectrum recorded at t = 5 min was used as the reference spectrum.

Time-courses of the peak area of the ν(OH) band and the peak position of the $\nu_{as}(CH_2)$ band during the ptBLM formation are shown in **Fig. 3c**. The $\nu_{as}(CH_2)$ peak shifted from 2923 to 2920 cm^{-1} after the removal of DDM. The wavenumber at 2920 cm^{-1} is quite close to that for the well-ordered alkyl chains (2918 cm^{-1}) [33], indicating that the densely packed ptBLM formed on the mixed SAM after the surfactant–lipid exchange. The peak area of the negative-going ν(OH) band also increased after the removal of DDM. Thus, the rapid removal of water molecules from the electrolyte/gold interface coupling with the densely packing of DMPC led to the assembly of the densely packed ptBLM. Interestingly, the ptBLM formation was completed in 10 min. This ptBLM formation process was much quicker than those for other ptBLM systems containing different membrane proteins: C*c*O (Complex IV) for ca. 1 h [13,14] and Complex I for ca. 10 h [15]. These proteins were immobilized on the gold surface *via* a nickel nitrilotriacetic acid (Ni-NTA) containing SAM, which could give different hydrogen bond networks of water molecules at the electrolyte/gold interface or different protein orientations. These differences can modulate interactions between phospholipid molecules and hydrophobic domains of the protein used.

3.3. Tracking of the BLM formation in the absence of cNOR on SAM/Au

For comparison, the BLM formation on the SAM/Au was also tracked in the absence of the cNOR (**Fig. 4**). The surfactant–lipid exchange caused the peak shift of $\nu_{as}(CH_2)$ from 2928 to 2920 cm^{-1} and the increase of the peak area of the negative-going band of ν(OH) over ca. 1 h (**Fig. 4c**). The BLM more slowly formed in the absence of the cNOR than the ptBLM in the presence of the cNOR (<10 min). The lipid−protein interaction between DMPC and the cNOR affected the kinetics of the lipid bilayer formation even on the same SAM/Au. It is most likely that transmembrane-spanning hydrophobic domains of the cNOR interact with the alkyl chains of DMPC *via* hydrophobic interactions [1-4,9-11] and then the ptBLM forms centered at the cNOR immobilized on the surface. The immobilized cNOR could serve as the nucleation center for the ptBLM assembly on the SAM/Au surface.

The protein-assisted nucleation mechanism for the ptBLM assembly was supported by the difference in the initial wavenumber of $\nu_{as}(CH_2)$ of DMPC. The initial wavenumber of $\nu_{as}(CH_2)$ at 2928 cm^{-1} for the BLM in the absence of the cNOR was higher than that at 2923 cm^{-1} for the ptBLM. This difference implies that the loosely packed lipid

bilayer was already reconstituted even in the presence of the surfactant thanks to the protein–lipid interactions. Note that the finally reached wavenumber of $\nu_{as}(CH_2)$ at 2920 cm^{-1} for the BLM in the absence of the cNOR was the same as that for the ptBLM, indicating that the presence and absence of the cNOR did not affect the final packing state of the lipid bilayer, in other words, the membrane fluidity [57]. No impact of the protein–lipid interaction on the peak shift of $\nu_{as}(CH_2)$ was also observed for a tethered-BLM with a bacterial respiratory membrane protein of ubiquinol/cytochrome bo_3 [38]. Thus, protein−lipid interactions play an important role in the BLM assembly kinetics on the SAM/Au but not the fluidity of the lipid bilayer membrane.

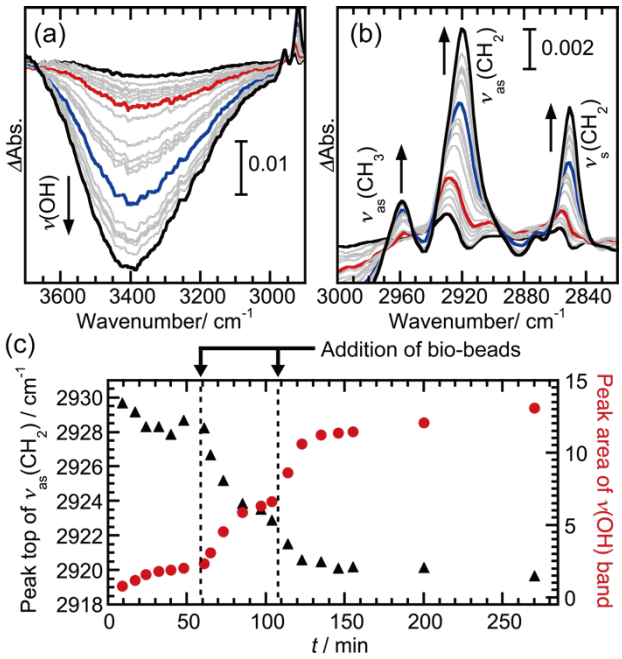

Fig. 4 Differential SEIRA spectra of the BLM formation on the 1:3 MPL–MPA mixed SAM/Au surface in the absence of *c*NOR (a) in the OH stretching region and (b) in the CH_3 and CH_2 stretching region. The traces in red and blue show the spectra just after the first and second additions of bio-beads, respectively. (c) Time-course of the peak top position of the CH_2 stretching vibration mode (the triangles in black) and the peak area of OH stretching band (the circles in red). DMPC was added into the solution at t = 0 min and Bio-beads were added at t = 60 and 110 min. A polarization-modulated spectrum recorded at t = 5 min was used as the reference spectrum.

The assembly process of the BLM and ptBLM on the mixed SAM/Au is summarized in **Fig. 5**. In the absence of the cNOR, the surfactant–lipid exchange initiated the slow BLM formation coupled with the removal of water molecules from the electrolyte/SAM interface over 1 h (**Fig. 5a**). In the presence of the cNOR, DMPC lipid molecules interact with the cNOR on the electrode and form the loosely packed lipid bilayer even in the presence of surfactants. The removal of surfactants immediately gave the densely packed ptBLM in 10 min (**Fig. 5b**).

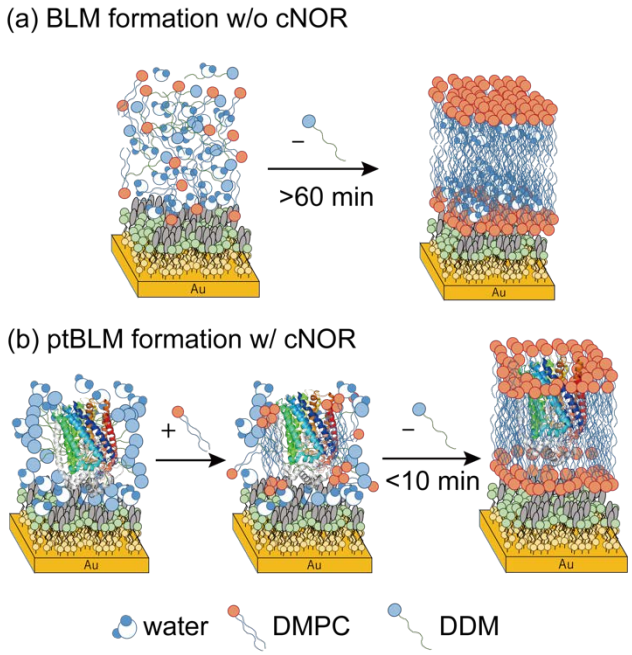

Fig. 5 Schematic representation of the formation of (a) the BLM in the absence of the cNOR and (b) the ptBLM in the presence of the cNOR on the mixed SAM-coated gold substrates.

3.4. Impact of the BLM on the enzymatic activity of the cNOR immobilized on the SAM/Au

To understand the effects of the protein–lipid interactions on the electrocatalytic activity of the cNOR, linear sweep voltammograms of the *c*NOR/SAM/Au electrode with or without the BLM were recorded under Ar and NO (**Fig. 6**). The cNOR/SAM/Au electrodes without the BLM showed cathodic currents under NO but not under Ar, indicating that the cNOR showed NO reduction activity [12,17]. Both electrodes showed the almost same onset potential at ca. –0.35 V vs. SHE. Thus, the lipid bilayer of DMPC showed no allosteric modulation of the electrocatalytic activity of the cNOR on the mixed SAM/Au. The electrocatalytic activity of metalloenzymes including the cNOR is known to highly depend on the protein orientation on the electrode surface

[12,19,58-60]. Since the protein orientation of the cNOR was fixed by covalent bonding with the SAM in this work, the protein orientation on the electrode was not changed by the ptBLM formation, resulting in almost no impact of the protein−lipid interaction on the electrocatalytic activity of the cNOR on the electrode. Note that the ptBLM electrode showed lower current densities at ca. –0.5 V vs. SHE (**Fig. 6**). The suppression of current densities for the ptBLM was caused by the limitation of the mass transport of NO from the electrolyte solution to the catalytic active site of the cNOR *via* lipid membranes [61]. Although almost no impact of the protein–lipid interaction for a model lipid of DMPC was observed on the electrocatalytic activity of the cNOR, the reconstitution of a surfactant-solubilized cNOR, which was isolated from *P. denitrificans*, into proteoliposomes containing lipids is known to improve the enzymatic activity as well as stability [62]. Since extracted soybean lipids or a mixture of synthetic lipids that mimic the original cellular membrane were used in the proteoliposomes, specific lipids could give the positive impact on the enzymatic activity of the cNOR in ptBLMs.

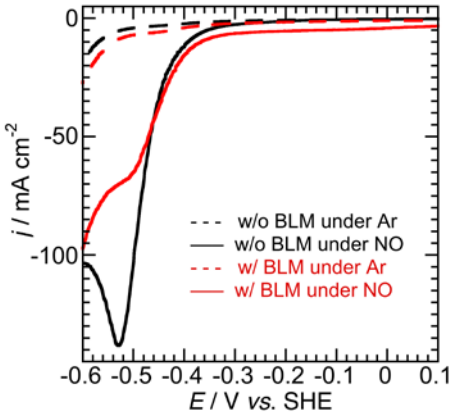

Fig. 6 Linear sweep voltammograms of the cNOR/SAM/Au electrode in the presence (in red) and absence (in black) of the BLM of DMPC under Ar (the broken traces) and NO (the solid traces). All voltammograms were recorded at a sweep rate of 20 mV s^{-1} in 50 mM MES-buffered electrolyte solution in D_2O containing 50 mM K_2SO_4 (pD 6.5).

Interestingly, cNOR/SAM/Au in the absence of the lipid bilayer showed more drastic changes in current densities for the NO reduction during potential cycles in the electrocatalytic condition than the ptBLM(cNOR)/SAM/Au (**Fig. 7**). This result implies that the presence of the lipid bilayer could improve the electrocatalytic stability of the immobilized cNOR. Thus, the protein−lipid interaction could improve the electrocatalytic stability but not the activity of the immobilized cNOR in this system.

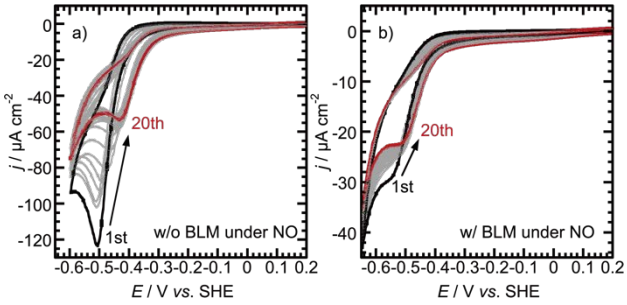

Fig. 7 A series of 20 consecutive cyclic voltammograms of (a) cNOR/SAM/Au and (b) ptBLM(cNOR)/SAM/Au recorded at 20 mV s^{-1} in 50 mM MES-buffered electrolyte solution in D_2O containing 50 mM K_2SO_4 (pD 6.5) under NO. The 1st and 20th cyclic voltammograms are shown in black and red, respectively.

4. Conclusions

The processes of the cNOR immobilization on the mixed SAM of 3:1 MPA–MPL and the ptBLM formation were studied by time-resolved SEIRA spectroscopy. To the mixed SAM/Au surface, α-helices that span the transmembrane region of the cNOR were vertically oriented. The formation of the densely packed ptBLM was coupled with the removal of water molecules from the SAM/Au interface. The comparison with the BLM formation process in the absence of the cNOR revealed that the protein−lipid interaction

between the cNOR and the DMPC phospholipid affected the assembly kinetics of the bilayer lipid membrane but not the fluidity. The BLM supported on the SAM/Au formed more slowly than the ptBLM. It seems that the ptBLM formation process highly depends on not only the protein–lipid interaction but also the nature of the SAM used [13-15]. More detailed studies on the impact of hydrophobicity and hydrophilicity of SAMs with different chain lengths and terminal groups on the ptBLM formation process are underway in our group.

Our work would stimulate further effort in the fundamental research of supported BLMs and PFE of redox-active membrane metalloproteins in biology and biological applications of ptBLMs.

Acknowledgments

The authors thank Shingo Mukai, Katsuhisa Ishikawa, Takahiko Hasegawa, and Yusuke Kawamura (Technical Division, Institute for Catalysis, Hokkaido University) for their technical supports on the experimental setup for the SEIRA spectroscopy. This work was supported by Grant-in-Aid for Young Scientists (B) (No. 16K20882 to M.K.),

Scientific Research (B) (No. 19H02664 to IY) and a MEXT Program for Development of Environmental Technology using Nanotechnology from the Ministry of Education, Culture, Sports, Science and Technology, Japan.

References

[1] J.R. Bolla, M.T. Agasid, S. Mehmood, C.V. Robinson, Membrane Protein–Lipid Interactions Probed Using Mass Spectrometry, Annual Review of Biochemistry, 88 (2019) 85-111.

[2] J. Flores, B.M. White, R.J. Brea, J.M. Baskin, N.K. Devaraj, Lipids: chemical tools for their synthesis, modification, and analysis, Chem. Soc. Rev., 49 (2020) 4602-4614.

[3] T. Gil, J.H. Ipsen, O.G. Mouritsen, M.C. Sabra, M.M. Sperotto, M.J. Zuckermann, Theoretical analysis of protein organization in lipid membranes, Biochimica et Biophysica Acta (BBA) - Reviews on Biomembranes, 1376 (1998) 245-266.

[4] O.S. Andersen, I. Roger E. Koeppe, Bilayer Thickness and Membrane Protein Function: An Energetic Perspective, Annual Review of Biophysics and Biomolecular Structure, 36 (2007) 107-130.

[5] D. Bizzotto, I.J. Burgess, T. Doneux, T. Sagara, H.-Z. Yu, Beyond Simple Cartoons: Challenges in Characterizing Electrochemical Biosensor Interfaces, ACS Sensors, 3 (2018) 5-12.

[6] N. Kornienko, K.H. Ly, W.E. Robinson, N. Heidary, J.Z. Zhang, E. Reisner, Advancing Techniques for Investigating the Enzyme–Electrode Interface, Acc. Chem. Res., 52 (2019) 1439-1448.

[7] M. Kato, J.Z. Zhang, N. Paul, E. Reisner, Protein film photoelectrochemistry of the water oxidation enzyme photosystem II, Chem. Soc. Rev., 43 (2014) 6485-6497.

[8] P.A. Ash, K.A. Vincent, Spectroscopic analysis of immobilised redox enzymes under direct electrochemical control, Chem. Commun., 48 (2012) 1400-1409.

[9] P.O. Saboe, E. Conte, M. Farell, G.C. Bazan, M. Kumar, Biomimetic and bioinspired approaches for wiring enzymes to electrode interfaces, Energy Environ. Sci., 10 (2017) 14-42.

[10] T. Laftsoglou, L.J.C. Jeuken, Supramolecular electrode assemblies for bioelectrochemistry, Chem. Commun., 53 (2017) 3801-3809.

[11] Z. Su, J.J. Leitch, J. Lipkowski, Electrode-supported biomimetic membranes: An electrochemical and surface science approach for characterizing biological cell membranes, Current Opinion in Electrochemistry, 12 (2018) 60-72.

[12] M. Kato, S. Nakagawa, T. Tosha, Y. Shiro, Y. Masuda, K. Nakata, I. Yagi, Surface-Enhanced Infrared Absorption Spectroscopy of Bacterial Nitric Oxide Reductase under

Electrochemical Control Using a Vibrational Probe of Carbon Monoxide, J. Phys. Chem. Lett., 9 (2018) 5196-5200.
[13] K. Ataka, F. Giess, W. Knoll, R. Naumann, S. Haber-Pohlmeier, B. Richter, J. Heberle, Oriented Attachment and Membrane Reconstitution of His-Tagged Cytochrome c Oxidase to a Gold Electrode: In Situ Monitoring by Surface-Enhanced Infrared Absorption Spectroscopy, J. Am. Chem. Soc., 126 (2004) 16199-16206.
[14] K. Ataka, B. Richter, J. Heberle, Orientational Control of the Physiological Reaction of Cytochrome c Oxidase Tethered to a Gold Electrode, J. Phys. Chem. B, 110 (2006) 9339-9347.
[15] S. Kriegel, T. Uchida, M. Osawa, T. Friedrich, P. Hellwig, Biomimetic Environment to Study E. coli Complex I through Surface-Enhanced IR Absorption Spectroscopy, Biochemistry, 53 (2014) 6340-6347.
[16] F. Melin, H. Xie, T. Meyer, Y.O. Ahn, R.B. Gennis, H. Michel, P. Hellwig, The unusual redox properties of C-type oxidases, Biochim. Biophys. Acta –Bioenergetics, 1857 (2016) 1892-1899.
[17] C.M. Cordas, A.G. Duarte, J.J.G. Moura, I. Moura, Electrochemical behaviour of bacterial nitric oxide reductase—Evidence of low redox potential non-heme FeB gives new perspectives on the catalytic mechanism, Biochim. Biophys. Acta –Bioenergetics, 1827 (2013) 233-238.
[18] X. Wang, R. Clément, M. Roger, M. Bauzan, I. Mazurenko, A.d. Poulpiquet, M. Ilbert, E. Lojou, Bacterial Respiratory Chain Diversity Reveals a Cytochrome c Oxidase Reducing O2 at Low Overpotentials, J. Am. Chem. Soc., 141 (2019) 11093-11102.
[19] M. Kato, T. Cardona, A.W. Rutherford, E. Reisner, Covalent Immobilization of Oriented Photosystem II on a Nanostructured Electrode for Solar Water Oxidation, J. Am. Chem. Soc., 135 (2013) 10610-10613.
[20] M. Kato, T. Cardona, A.W. Rutherford, E. Reisner, Photoelectrochemical Water Oxidation with Photosystem II Integrated in a Mesoporous Indium–Tin Oxide Electrode, J. Am. Chem. Soc., 134 (2012) 8332-8335.
[21] K.P. Sokol, D. Mersch, V. Hartmann, J.Z. Zhang, M.M. Nowaczyk, M. Rögner, A. Ruff, W. Schuhmann, N. Plumeré, E. Reisner, Rational wiring of photosystem II to hierarchical indium tin oxide electrodes using redox polymers, Energy Environ. Sci., 9 (2016) 3698-3709.
[22] X. Fang, K.P. Sokol, N. Heidary, T.A. Kandiel, J.Z. Zhang, E. Reisner, Structure–

Activity Relationships of Hierarchical Three-Dimensional Electrodes with Photosystem II for Semiartificial Photosynthesis, Nano Lett., 19 (2019) 1844-1850.
[23] J. Kozuch, C. Steinem, P. Hildebrandt, D. Millo, Combined Electrochemistry and Surface-Enhanced Infrared Absorption Spectroscopy of Gramicidin A Incorporated into Tethered Bilayer Lipid Membranes, Angew. Chem. Int. Ed., 51 (2012) 8114-8117.
[24] F. Melin, P. Hellwig, Recent advances in the electrochemistry and spectroelectrochemistry of membrane proteins, Biological Chemistry, 394 (2013) 593.
[25] C. Steininger, C. Reiner-Rozman, A. Schwaighofer, W. Knoll, R.L.C. Naumann, Kinetics of cytochrome c oxidase from R. sphaeroides initiated by direct electron transfer followed by tr-SEIRAS, Bioelectrochemistry, 112 (2016) 1-8.
[26] C. Nowak, M.G. Santonicola, D. Schach, J. Zhu, R.B. Gennis, S. Ferguson-Miller, D. Baurecht, D. Walz, W. Knoll, R.L.C. Naumann, Conformational transitions and molecular hysteresis of cytochrome c oxidase: Varying the redox state by electronic wiring, Soft Matter, 6 (2010) 5523-5532.
[27] X. Jiang, E. Zaitseva, M. Schmidt, F. Siebert, M. Engelhard, R. Schlesinger, K. Ataka, R. Vogel, J. Heberle, Resolving voltage-dependent structural changes of a membrane photoreceptor by surface-enhanced IR difference spectroscopy, Proc. Natl. Acad. Sci. U.S.A., 105 (2008) 12113-12117.
[28] F.O. Gomes, L.B. Maia, J.A. Loureiro, M.C. Pereira, C. Delerue-Matos, I. Moura, J.J.G. Moura, S. Morais, Biosensor for direct bioelectrocatalysis detection of nitric oxide using nitric oxide reductase incorporated in carboxylated single-walled carbon nanotubes/lipidic 3 bilayer nanocomposite, Bioelectrochemistry, 127 (2019) 76-86.
[29] F.O. Gomes, L.B. Maia, C. Delerue-Matos, I. Moura, J.J.G. Moura, S. Morais, Third-generation electrochemical biosensor based on nitric oxide reductase immobilized in a multiwalled carbon nanotubes/1-n-butyl-3-methylimidazolium tetrafluoroborate nanocomposite for nitric oxide detection, Sensors and Actuators B: Chemical, 285 (2019) 445-452.
[30] M. Duca, M.T.M. Koper, Powering denitrification: the perspectives of electrocatalytic nitrate reduction, Energy Environ. Sci., 5 (2012) 9726-9742.
[31] K. Ataka, S.T. Stripp, J. Heberle, Surface-enhanced infrared absorption spectroscopy (SEIRAS) to probe monolayers of membrane proteins, Biochim. Biophys. Acta – Biomembranes, 1828 (2013) 2283-2293.
[32] Á.I. López-Lorente, C. Kranz, Recent advances in biomolecular vibrational

spectroelectrochemistry, Current Opinion in Electrochemistry, 5 (2017) 106-113.
[33] A. Quirk, M.J. Lardner, Z. Tun, I.J. Burgess, Surface-Enhanced Infrared Spectroscopy and Neutron Reflectivity Studies of Ubiquinone in Hybrid Bilayer Membranes under Potential Control, Langmuir, 32 (2016) 2225-2235.
[34] E. Forbrig, J.K. Staffa, J. Salewski, M.A. Mroginski, P. Hildebrandt, J. Kozuch, Monitoring the Orientational Changes of Alamethicin during Incorporation into Bilayer Lipid Membranes, Langmuir, 34 (2018) 2373-2385.
[35] A.F. Santos Seica, J. Schimpf, T. Friedrich, P. Hellwig, Visualizing the movement of the amphipathic helix in the respiratory complex I using a nitrile infrared probe and SEIRAS, FEBS Lett., 594 (2020) 491-496.
[36] H. Noguchi, T. Adachi, A. Nakatomi, M. Yazawa, K. Uosaki, Biofunctionality of Calmodulin Immobilized on Gold Surface Studied by Surface-Enhanced Infrared Absorption Spectroscopy: Ca2+-Induced Conformational Change and Binding to a Target Peptide, J. Phys. Chem. C, 120 (2016) 16035-16041.
[37] J. Kozuch, C. Weichbrodt, D. Millo, K. Giller, S. Becker, P. Hildebrandt, C. Steinem, Voltage-dependent structural changes of the membrane-bound anion channel hVDAC1 probed by SEIRA and electrochemical impedance spectroscopy, Phys. Chem. Chem. Phys., 16 (2014) 9546-9555.
[38] S. Wiebalck, J. Kozuch, E. Forbrig, C.C. Tzschucke, L.J.C. Jeuken, P. Hildebrandt, Monitoring the Transmembrane Proton Gradient Generated by Cytochrome bo3 in Tethered Bilayer Lipid Membranes Using SEIRA Spectroscopy, J. Phys. Chem. B, 120 (2016) 2249-2256.
[39] A.K. Covington, M. Paabo, R.A. Robinson, R.G. Bates, Use of the glass electrode in deuterium oxide and the relation between the standardized pD (paD) scale and the operational pH in heavy water, Anal. Chem., 40 (1968) 700-706.
[40] T. Hino, Y. Matsumoto, S. Nagano, H. Sugimoto, Y. Fukumori, T. Murata, S. Iwata, Y. Shiro, Structural Basis of Biological N2O Generation by Bacterial Nitric Oxide Reductase, Science, 330 (2010) 1666-1670.
[41] E. Terasaka, K. Yamada, P.H. Wang, K. Hosokawa, R. Yamagiwa, K. Matsumoto, S. Ishii, T. Mori, K. Yagi, H. Sawai, H. Arai, H. Sugimoto, Y. Sugita, Y. Shiro, T. Tosha, Dynamics of nitric oxide controlled by protein complex in bacterial system, Proc Natl Acad Sci U S A, 114 (2017) 9888-9893.
[42] H. Miyake, S. Ye, M. Osawa, Electroless deposition of gold thin films on silicon for

surface-enhanced infrared spectroelectrochemistry, Electrochem. Commun., 4 (2002) 973-977.
[43] M. Yaguchi, T. Uchida, K. Motobayashi, M. Osawa, Speciation of Adsorbed Phosphate at Gold Electrodes: A Combined Surface-Enhanced Infrared Absorption Spectroscopy and DFT Study, J. Phys. Chem. Lett., 7 (2016) 3097-3102.
[44] M. Kato, K. Ogura, S. Nakagawa, S. Tokuda, K. Takahashi, T. Nakamura, I. Yagi, Enhancement of Electrocatalytic Oxygen Reduction Activity and Durability of Pt-Ni Rhombic Dodecahedral Nanoframes by Anchoring to Nitrogen-Doped Carbon Support, ACS Omega, 3 (2018) 9052-9059.
[45] K. Kunimatsu, K. Miyatake, S. Deki, H. Uchida, M. Watanabe, Analysis of the Gold/Polymer Electrolyte Membrane Interface by Polarization-Modulated ATR-FTIR Spectroscopy, J. Phys. Chem. C, 119 (2015) 16754-16761.
[46] B. Ge, F. Lisdat, Superoxide sensor based on cytochrome c immobilized on mixed-thiol SAM with a new calibration method, Anal. Chim. Acta, 454 (2002) 53-64.
[47] J. Grochol, R. Dronov, F. Lisdat, P. Hildebrandt, D.H. Murgida, Electron Transfer in SAM/Cytochrome/Polyelectrolyte Hybrid Systems on Electrodes: A Time-Resolved Surface-Enhanced Resonance Raman Study, Langmuir, 23 (2007) 11289-11294.
[48] A. Badura, B. Esper, K. Ataka, C. Grunwald, C. Wöll, J. Kuhlmann, J. Heberle, M. Rögner, Light-Driven Water Splitting for (Bio-)Hydrogen Production: Photosystem 2 as the Central Part of a Bioelectrochemical Device, Photochem. Photobiol., 82 (2006) 1385-1390.
[49] E.E. Ferapontova, T. Ruzgas, L. Gorton, Direct Electron Transfer of Heme- and Molybdopterin Cofactor-Containing Chicken Liver Sulfite Oxidase on Alkanethiol-Modified Gold Electrodes, Anal. Chem., 75 (2003) 4841-4850.
[50] M. Sezer, R. Spricigo, T. Utesch, D. Millo, S. Leimkuehler, M.A. Mroginski, U. Wollenberger, P. Hildebrandt, I.M. Weidinger, Redox properties and catalytic activity of surface-bound human sulfite oxidase studied by a combined surface enhanced resonance Raman spectroscopic and electrochemical approach, Phys. Chem. Chem. Phys., 12 (2010) 7894-7903.
[51] M. Sezer, P. Kielb, U. Kuhlmann, H. Mohrmann, C. Schulz, D. Heinrich, R. Schlesinger, J. Heberle, I.M. Weidinger, Surface Enhanced Resonance Raman Spectroscopy Reveals Potential Induced Redox and Conformational Changes of Cytochrome c Oxidase on Electrodes, J. Phys. Chem. B, 119 (2015) 9586-9591.

[52] A. Barth, Infrared spectroscopy of proteins, Biochim. Biophys. Acta –Bioenergetics, 1767 (2007) 1073-1101.
[53] T. Hino, Y. Matsumoto, S. Nagano, H. Sugimoto, Y. Fukumori, T. Murata, S. Iwata, Y. Shiro, Structural Basis of Biological N₂O Generation by Bacterial Nitric Oxide Reductase, Science, 330 (2010) 1666-1670.
[54] T. Uchida, M. Osawa, J. Lipkowski, SEIRAS studies of water structure at the gold electrode surface in the presence of supported lipid bilayer, J. Electroanal. Chem., 716 (2014) 112-119.
[55] S. Yukari, F.B. L., C.R. M., U. Kohei, Polarization Modulation Fourier Transform Infrared Studies of the Effects of Self-Assembly Time on the Order and Orientation of 11-Ferrocenyl-1-undecanethiol Monolayers on Gold, Bulletin of the Chemical Society of Japan, 67 (1994) 21-25.
[56] O. Gutiérrez-Sanz, E. Forbrig, A.P. Batista, M.M. Pereira, J. Salewski, M.A. Mroginski, R. Götz, A.L. De Lacey, J. Kozuch, I. Zebger, Catalytic Activity and Proton Translocation of Reconstituted Respiratory Complex I Monitored by Surface-Enhanced Infrared Absorption Spectroscopy, Langmuir, 34 (2018) 5703-5711.
[57] B. Khairalla, J. Juhaniewicz-Debinska, S. Sek, I. Brand, The shape of lipid molecules affects potential-driven molecular-scale rearrangements in model cell membranes on electrodes, Bioelectrochemistry, 132 (2020) 107443.
[58] O. Rüdiger, J.M. Abad, E.C. Hatchikian, V.M. Fernandez, A.L. De Lacey, Oriented Immobilization of Desulfovibrio gigas Hydrogenase onto Carbon Electrodes by Covalent Bonds for Nonmediated Oxidation of H2, J. Am. Chem. Soc., 127 (2005) 16008-16009.
[59] P. Olejnik, B. Palys, A. Kowalczyk, A.M. Nowicka, Orientation of Laccase on Charged Surfaces. Mediatorless Oxygen Reduction on Amino- and Carboxyl-Ended Ethylphenyl Groups, J. Phys. Chem. C, 116 (2012) 25911-25918.
[60] J. Liu, Y. Xie, C. Peng, G. Yu, J. Zhou, Molecular Understanding of Laccase Adsorption on Charged Self-Assembled Monolayers, J. Phys. Chem. B, 121 (2017) 10610-10617.
[61] E. Terasaka, K. Yamada, P.-H. Wang, K. Hosokawa, R. Yamagiwa, K. Matsumoto, S. Ishii, T. Mori, K. Yagi, H. Sawai, H. Arai, H. Sugimoto, Y. Sugita, Y. Shiro, T. Tosha, Dynamics of nitric oxide controlled by protein complex in bacterial system, Proc. Natl. Acad. Sci. U.S.A., 114 (2017) 9888-9893.
[62] J. ter Beek, M. Kahle, P. Adelroth, Modulation of protein function in membrane

mimetics: Characterization of P. denitrificans cNOR in nanodiscs or liposomes, Boichim. Biophys. Acta-Biomembranes, 1859 (2017) 1951-1961.